ACS ES&T Water

pubs.acs.org/estwater

Article

Leveraging Multiple Raman Excitation Wavelength Systems for Process Monitoring of Nuclear Waste Streams

Heather M. Felmy, Hope E. Lackey, Adan Schafer Medina, Michael J. Minette, Samuel A. Bryan,* and Amanda M. Lines*

Cite This: https://doi.org/10.1021/acsestwater.1c00408

Read Online

ACCESS | Metrics & More | Article Recommendations | Supporting Information

ABSTRACT: Processing nuclear waste from sites such as Hanford is a significant environmental cleanup need while being a significant logistical challenge. Integration of process monitoring tools, which can provide *in situ* and real-time feedback about the process, can significantly alleviate needs to collect grab samples for process control and product characterization. Raman spectroscopy paired with chemometric analysis is one process monitoring tool that can provide chemical composition information on a large number of chemical targets in nuclear waste streams. However, methods to improve limits of detection as well as drop uncertainty in quantification are needed. Optimizing instrument specifications can achieve this; here, this is demonstrated by comparing limits of detection for key analytes when using Raman systems with 671, 532, and 405 nm excitation wavelengths. Generally, limits of detection decrease (allowing the measurement of lower salt concentrations) with decreasing wavelength. Similarly, data collection times and averaging were optimized. Finally, multiple chemometric modeling approaches were leveraged, including multiblock methods that combined data from all three Raman systems to simultaneously quantify targets with improved sensitivity.

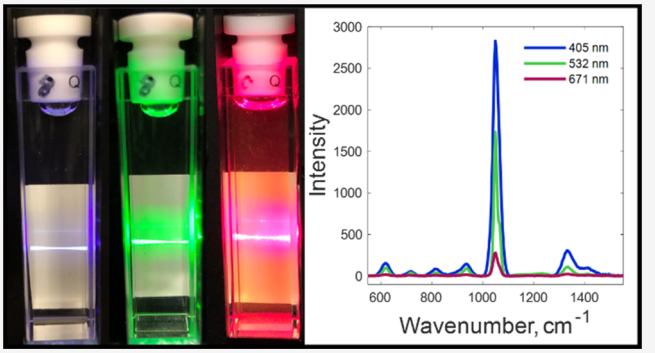

KEYWORDS: *online monitoring, chemometric modeling, Raman spectroscopy, Hanford, partial least-squares (PLS) regression*

INTRODUCTION

The Hanford site is a 560 square mile former plutonium production site located along the Columbia River, which comprises the north and east borders of the nuclear reservation.[1] The nuclear reactors and plutonium reprocessing plants have been closed and are decommissioned. Much of the waste generated from the reprocessing of the nuclear fuel process has been deposited within 177 single- and double-shell, mild-steel-lined tanks, the largest of which hold ~1 M gallons of radioactive waste. The waste, prior to being placed in the tanks, were neutralized with sodium hydroxide to prevent corrosion of the mild-steel liners. Several of these tanks have been confirmed to have leaked, and all of the single-shell tanks (149) are considered to have exceeded their design life. It is estimated that approximately 150 square miles of groundwater has been contaminated at Hanford, with greater than 400 billion gallons of liquids, some containing radionuclides and hazardous chemicals, have been released to the ground/vadose zone since 1944.[1] The concern is with how much or if any of this contamination has reached the groundwater. This work is designed to aid in the quantitative analysis of the chemical species contained within the radioactive waste.

Process monitoring, or real-time and *in situ* process characterization, is the optimal route to provide comprehensive and continuous analysis of chemical systems. This includes flow or batch processes, with the intent for fundamental characterization or process optimization and control. Currently, on- or inline process monitoring techniques are used for numerous industrial-scale processing applications, including food and pharmaceutical industries, where they have enabled significant improvements in process control and reductions in process costs.[2−6] Numerous tools are commercially available and provide a range of process information; however, for process control and verification, analysis of chemical composition is particularly valuable.

Monitoring approaches based on optical spectroscopy are uniquely suited to providing detailed chemical composition information on a process batch or stream.[7−12] Optical approaches can provide a range of chemical information, including identification and quantification of elemental and molecular species.[9,13−16] Optical approaches are also generally

Received: October 21, 2021
Revised: January 13, 2022
Accepted: February 11, 2022

mature and can be flexibly integrated into a variety of process types.[13,17,18] As an example, optical spectroscopy probes can be plumbed into hazardous environments and are robust enough to withstand radiation dose, corrosive media, high temperatures, and wide ranges of pressures.[7,17−19] Most beneficially, for several optical approaches such as Raman, instrumentation and control equipment can be located in remote, safe locations with only fiber optics traversing the space between detectors and probes.

These techniques can be applied to low activity waste (LAW)[19] and, potentially, high-level waste (HLW) process streams at the Hanford site. The processing of materials from tank farms needs to be characterized to support compliance, corrosion control, and process control. Current plans focus on grab sample collection and offline analysis; however, integration of online monitoring can help operators reduce needs for sample collection, improve process time scales, and reduce characterization costs.

Raman spectroscopy can be particularly valuable because it can be used to uniquely identify and quantify numerous tank waste anions, including those that comprise the majority of tank waste by mass.[10,19,20] Raman technology is ideal for applications to *in situ* and real-time monitoring of tank processing streams because of the simple yet powerful way this form of spectroscopy works. Raman is a fast (<1−5 s measurement), nondestructive technique that relies on interrogating a system with an excitation laser and picking up the inelastically scattered light. An optical window or penetration port is all that is required to allow Raman interrogation of a stream. The Raman probe itself contains only optics and no electronics, which enables it to maintain a long functional lifetime in radiation and chemically harsh environments.[19] Raman spectroscopy can also be paired with multivariate analysis to enable real-time analysis of highly complex data.[9,13,14,21]

However, a significant gap can be found in the application of Raman approaches to very low-concentration waste streams. This can potentially be addressed by taking a two-pronged approach: (1) optimizing instrument parameters and (2) modifying data analysis approaches. Here, these approaches are explored. This includes utilizing and comparing responses for three Raman systems using 671 nm (red), 532 nm (green), and 405 nm (blue) excitation lasers. The decrease in excitation wavelength should increase sensitivity, but there is a tradeoff with increasing susceptibility to fluorescence background. Other optimized parameters include data collection specifications such as integration time and spectral averaging. Finally, a range of modeling approaches was explored, including multiblock or simultaneous characterization of data from all three Raman systems. Different modeling approaches produced varying degrees of uncertainty in outputs, with multiblock approaches showing good reduction of uncertainty or improved confidence in the accuracy of quantifying low-concentration samples.

EXPERIMENTAL SECTION

Materials. The following chemicals were used as purchased without further purification: NaOH (Ricca, 10.0 N), Al-$(NO_3)_3(H_2O)_9$ (Sigma-Aldrich, ≥98%), $NaAlO_2$ (Sigma-Aldrich), Na_2CO_3 (Sigma-Aldrich, ≥99.5%), $Na_2CrO_4(H_2O)_4$ (Sigma-Aldrich, 99%), $NaNO_3$ (Sigma-Aldrich, ≥99.0%), $NaNO_2$ (Sigma-Aldrich, ≥99.0%), $Na_3PO_4(H_2O)_{12}$ (Acros Organics, >98%), Na_2SO_4 (Sigma-Aldrich, ≥99%), $Na_2C_2O_4$ (Sigma-Aldrich, ≥99.5%), NH_4NO_3 (Acros Organics, >99%), and NH_4OH (J. T. Baker, 5 N).

Training set solutions consisted of 10−12 solutions of each analyte spanning the concentration ranges listed in Table 1. All analyte solutions also contained either 0.1 or 1 M excess NaOH to maintain high pH and better simulate the real tank samples. $Al(NO_3)_3$ and $NaAlO_2$ solutions were dissolved in enough excess NaOH to dissolve Al as $Al(OH)_4^-$. This training set was designed to capture the complex spectral variability including chemical interactions, band overlap, and potential baseline effects. This set was optimized for low uncertainty in concentration values to provide the highest fidelity quantification of validation set samples. The concentration range of each analyte was chosen to encompass the anticipated concentration range of the real processing samples. Following the collection of the training set samples, we were presented the opportunity to analyze more complex solutions including some simulants and real tank samples, some of which included analyte concentrations outside the training set concentration range. These were included in the analysis as a valuable demonstration of highly complex systems.

Table 1. Analyte Concentration Ranges for Solutions Prepared for the Training Set

analyte	concentration range (M)
NaOH	0.05−8
$Al(OH)_4^-$	0.001−1
CO_3^{2-}	0.01−2
CrO_4^{2-}	0.0005−1
NO_3^-	0.01−3
NO_2^-	0.01−1
PO_4^{3-}	0.0005−0.5
SO_4^{2-}	0.0005−0.75
$C_2O_4^{2-}$	0.0005−0.15
NH_4^+	0.005−5

The validation or test set was composed of three sets of samples: real tank processing samples, tank simulant samples, and additional validation samples with low analyte concentrations, designed to test the lower limit of the models. These additional validation samples consisted of 10 solutions containing mixtures of 4−9 analytes within the lower concentration ranges listed in Table 1. The concentrations of all test set samples are included in Table S1.

Instrumentation. Three Raman systems were utilized for this work. All were acquired from Spectra Solutions Inc. and included 405, 532, and 671 nm excitation lasers with adjustable laser power. Each spectrometer wavenumber reading was calibrated using naphthalene, and the resolution of each was <5 cm^{-1}. Each system was connected via fiber optic cables to a probe connected to a cuvette holder. The probe employs a miniature fiber optic Raman probe with a backscattering (180°) optical design. A high-throughput volume phase holographic (VPH) grating spectrograph with a TE-cooled two-dimensional CCD detector was used to record the Raman signal from the Raman probe. All samples were measured in a standard 1 cm quartz cuvette. An example of the sample measurement for the 532 nm system is shown in Figure 1.

Initial system optimization was conducted on the nitrate and oxalate samples by modifying the laser power of each system to maximize the signal. This was found to be approximately 35, 20, and 220 mW for the 405, 532, and 671 nm systems,

https://doi.org/10.1021/acsestwater.1c00408
ACS EST Water XXXX, XXX, XXX−XXX

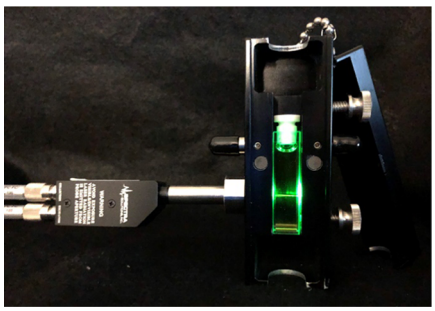

Figure 1. Raman probe (532 nm) illuminating a sample cuvette in a cuvette holder.

respectively. With these laser-power settings, the nitrate and oxalate samples were measured at 1, 2, 5, and 10 s integration times and using spectral averaging ranging from 1 to 100 to determine the effect of integration time and spectral averaging on the limit of detection (LOD) calculations to optimize those settings for additional measurements.

Further measurements on the entire training and validation set were performed by setting all laser powers to approximately 100 mW (80, 100, and 120 mW for the 405, 532, and 671 nm systems, respectively) and using an integration time of 0.5 s.

Chemometric Modeling. Chemometric models were generated using MATLAB (R2020b) with the Eigenvector Research PLS-Toolbox (version 8.9). Models were built by modeling each laser system separately and using multiblock modeling, which combines the data from all three systems into a single model. Cross validation for all models utilized the venetian blinds method with 10 data splits and 1 sample per blind. In this way, the models were tested on the ability to predict concentrations of training set samples left out of the model during cross validation. Spectral preprocessing consisted of the first derivative, normalization to the water band from ~2800 to 3800 cm^{-1}, followed by mean centering to account for any baseline shifts due to sample fluorescence. While the shape of the water band is affected by pH, in general, the area under the curve does not vary significantly with changes in pH because the concentration of water (55 M) does not change significantly with comparatively small changes in hydroxide concentration.[22] Therefore, it was decided to normalize to this band to account for any intensity changes due to laser-power fluctuations.

RESULTS AND DISCUSSION

Comparing and Optimizing Signatures between Raman Systems. Limits of detection (LOD) were used as a way of determining optimal system parameters. The LOD was compared based on several factors including spectral averaging, integration time, and laser-power settings. The concentration LOD was calculated from eq 1:

$$\mathrm{LOD} = \frac{3s}{m} \tag{1}$$

where s is the standard deviation of blank (solutions containing no analyte) measurements—in this case, water spectra, and m is the slope of the line obtained from plotting the peak intensity versus analyte concentration.[23]

The main experimental factors used for data collection optimization are laser wavelength, laser power, and integration time. Modifying laser power will impact the signal produced by each laser system, which can be useful for determining analyte spectral signatures. When trying to directly compare fingerprint characteristics or directly compare impacts of averaging/longer collection times, setting lasers to different settings that roughly result in equal signal intensities can be highly useful. Figure 2

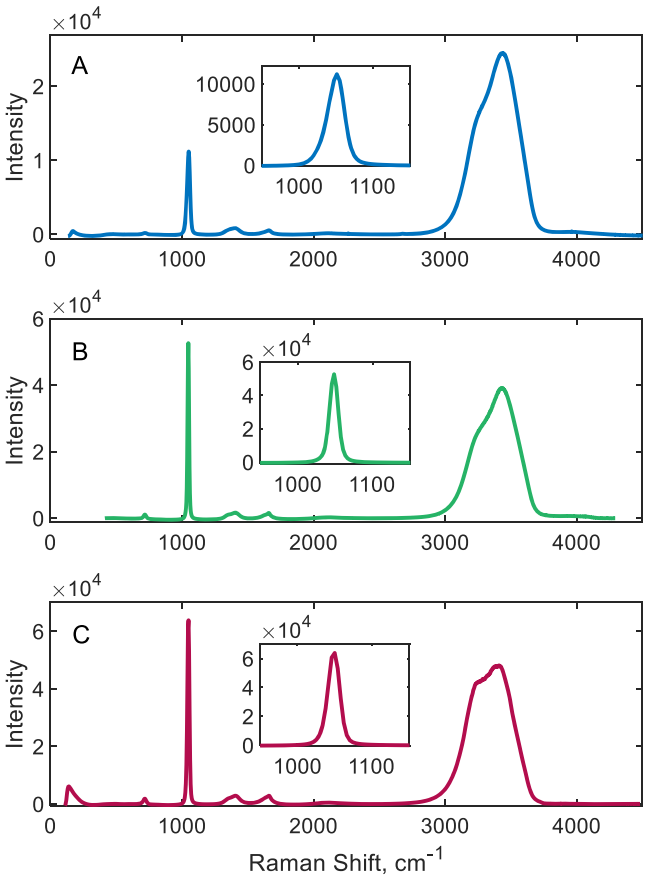

Figure 2. Spectral fingerprints of 3 M NO_3^- on the 405 nm (A), 532 nm (B), and 671 nm (C) systems with a 10 s integration time and an average of 100 spectra. The inset shows the nitrate band. Laser powers were approximately 35, 20, and 220 mW for the 405, 532, and 671 nm lasers, respectively. The spectra in this figure have been replotted on a common wavelength (absolute nm) scale to highlight the differences in Raman spectra collected with different wavelengths of excitation and are shown in Figure S1.

demonstrates this for a nitrate sample measured on each laser system at laser powers of 35, 20, and 220 mW for the 405, 532, and 671 nm systems, respectively. In comparing the spectra from the three laser systems, there is a noticeable difference in peak ratios between the water band around 3400 cm^{-1} and the nitrate band at 1050 cm^{-1}. Given the grating settings and response to the blue excitation wavelength, the nitrate band is significantly less intense but broader in the 405 nm system than the other two systems.

Nitrate (strong Raman response) and oxalate (weak Raman response) samples were measured at 1, 2, 5, and 10 s integration time at these laser powers (35, 20, and 220 mW for the 405, 532, and 671 nm systems, respectively) to study the effect of integration time on the calculated LOD. These LODs are presented in Table S2. Also included is a comparison of spectral averaging on the LOD. Increased averaging and integration time both increase the signal-to-noise ratio and improve the LOD, especially for low-signal analytes such as oxalate. Comparing the LODs, there was up to a 14×

https://doi.org/10.1021/acsestwater.1c00408
ACS EST Water XXXX, XXX, XXX−XXX

Table 2. Limits of Detection (LOD) in Molarity, M of Nitrate, and Oxalate with Optimized Settings of 0.5 s Integration Time and All Laser Systems Set to Approximately 100 mW, with Varying Spectral Averaging[a]

analyte	excitation wavelength (nm)	laser power (mW)	integration time (s)	average 1	average 5	average 10	average 50	average 100
NO_3^-	405	80	0.5	65.4×10^{-4}	22.2×10^{-4}	13.9×10^{-4}	2.88×10^{-4}	1.92×10^{-4}
	532	100	0.5	63.7×10^{-4}	40.3×10^{-4}	19.3×10^{-4}	6.05×10^{-4}	2.13×10^{-4}
	671	120	0.5	378×10^{-4}	194×10^{-4}	142×10^{-4}	42.0×10^{-4}	21.5×10^{-4}
$C_2O_4^{2-}$	405	80	0.5	392×10^{-4}	128×10^{-4}	132×10^{-4}	59.3×10^{-4}	8.79×10^{-4}
	532	100	0.5	610×10^{-4}	441×10^{-4}	213×10^{-4}	37.5×10^{-4}	16.8×10^{-4}
	671	120	0.5	1600×10^{-4}	674×10^{-4}	618×10^{-4}	222×10^{-4}	37.0×10^{-4}

[a]Spectral preprocessing consisted of the first derivative, normalization to the water band, followed by mean centering.

improvement in calculated LOD for oxalate by increasing the integration time from 1 to 10 s, and there was a 72× improvement by increasing the averaging from 1 to 10 spectra. By increasing the averaging from 1 to 100 spectra, there was up to a 2000× improvement in oxalate LOD. While increasing the averaging can significantly improve the measurement, this requires the collection of more spectra, which increases the data collection time. Increasing the integration time not only improves the LOD but also increases the time required to collect the data, and the maximum integration time will be limited by the detector's maximum range before reaching saturation. Note, when choosing optimum collection times and averaging numbers for online applications, operators must find a balance between improved limits of detection (long times for data collection) and information output needs (frequent vs infrequent data output). Here, to achieve the needed output, frequency data collection parameters were set to 0.5 s integration time and spectral averaging of 100.

While modifying laser power to maximize signals is useful when directly comparing laser systems, it does not provide good insight into the true performance capabilities of each instrument. It was therefore determined that the best comparison would be made by setting all laser powers to the same setting (approximately 100 mW) and using the same integration time (0.5 s), where 0.5 s was the highest integration time possible before saturating the 405 nm system. While this is a very low integration time compared to the best response (10 s listed in Table S2), it was used to maintain shorter experiment times and allow for matrix fusion of data sets with consistent timing outputs. This loss of signal-to-noise ratio can also be compensated for by increasing the averaging, as averaging was found to have a greater influence on LOD than integration time.

The LODs for the nitrate and oxalate samples using these optimized settings are presented in Table 2, and examples of nitrate spectra using these optimized settings are shown in Figure S2.

Collecting Training Sets and Chemometric Model Building. Many of the key analytes in the Hanford tanks are Raman active. The Raman fingerprints of several of these analytes are shown in Figure 3 for each laser system. While many of the spectral signatures are similar between the different wavelength laser systems, the intensities and ratio between peaks are slightly different. Noticeably absent from the 405 nm system is the CrO_4^{2-} band. This is due to the absorbance of the laser light. The absorbance spectra of these analytes are shown in Figure S3. Several analytes absorb at lower wavelengths, and most relevant to this study is the strong absorbance of CrO_4^{2-} below about 510 nm, essentially completely absorbing the 405 nm laser. This is an example

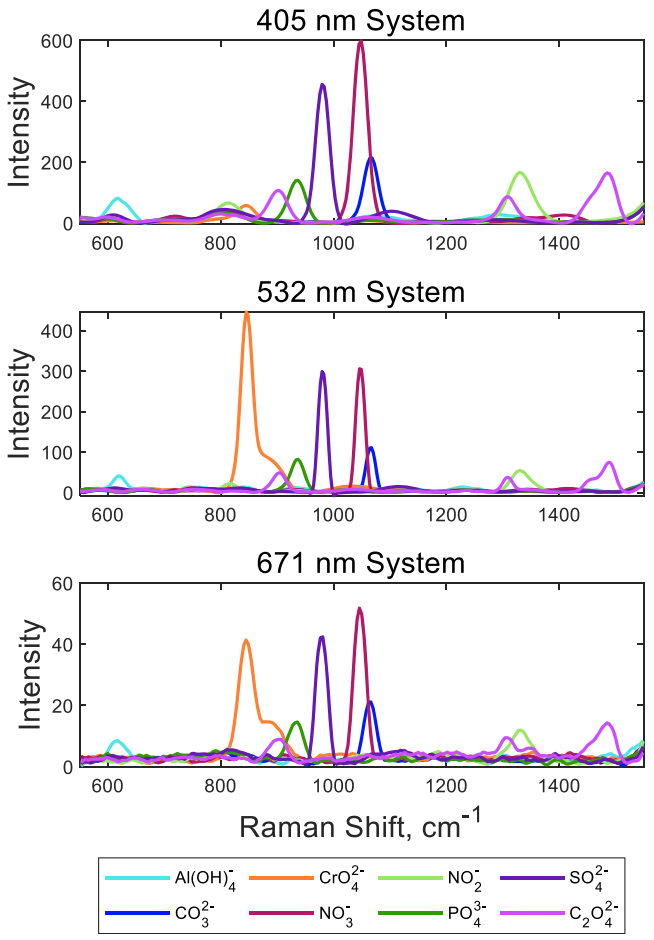

Figure 3. Spectral fingerprints of key analytes in the training set measured with the 405 nm (A), 532 nm, (B) and 671 nm (C) systems. Each spectrum represents an average of 100 spectra and 0.1 M analyte concentration, except CrO_4^{2-}, which is shown at 0.01 M due to a significantly higher signal. The spectra in this figure have been replotted on a common wavelength (absolute nm) scale to highlight the differences in Raman spectra collected with different wavelengths of excitation and are shown in Figure S4.

of the tradeoff between the higher signal and higher sensitivity of lower wavelength lasers versus the stronger absorbance and loss of Raman signal for some species.

The absorption of the 405 nm laser light by the chromate chromophore increases the potential for observing a resonance Raman effect (RRE) in this system. Indeed, other researchers have measured the RRE and pre-RRE using variable wavelengths using various argon-ion laser lines for excitation. The highest RRE enhancement was observed using 363.8 and 351.1

https://doi.org/10.1021/acsestwater.1c00408
ACS EST Water XXXX, XXX, XXX−XXX

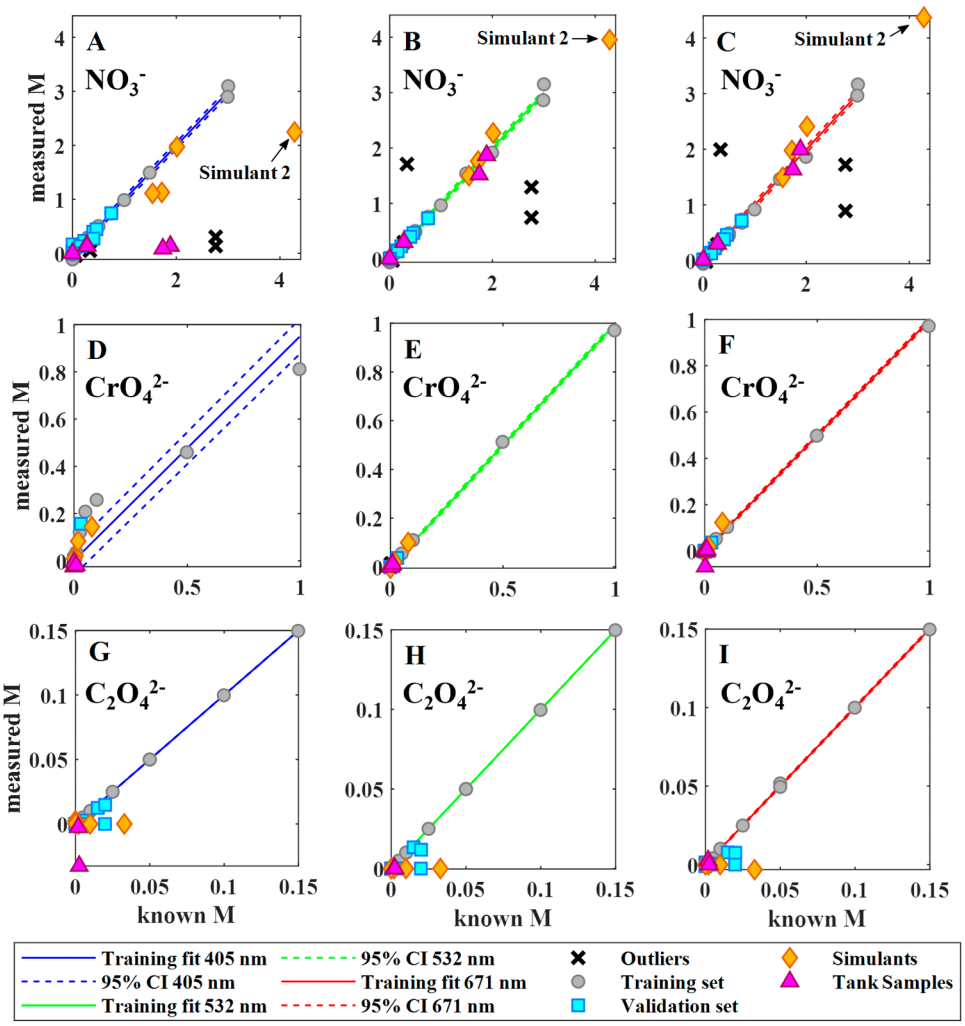

Figure 4. Parity plots from modeling each laser system separately for the nitrate (A–C), chromate (D–F), and oxalate (G–I) systems using the 405 nm (A, D, G), 532 nm (B, E, H), and 671 nm (C, F, I) data.

nm (ultraviolet) excitation, which were close to the λ_{max} absorption for chromate at 370 nm. Wavelengths used for Raman excitation lower than the λ_{max} absorption (in the visible region) resulted in weaker pre-RRE enhancement.[24] In our work, an enhancement for the chromate ion measurement was not observed owing to the excitation wavelength being in the visible (pre-RRE) region and due to absorption/reabsorption of the laser light/Raman emission in the samples containing chromate ions. The effect of the absorption of the 405 nm laser light on modeling is discussed in a subsequent section.

Several chemometric modeling approaches were explored for this system. Partial least-squares (PLS) regression was the primary algorithmic approach utilized. This technique has been applied to other studies of complex systems,[14,19,25] and mechanics have been discussed elsewhere.[26,27] To add further robustness in handling complex data (overlapping or interfering signatures from multicomponent samples[28]), several models leveraging locally weighted regression were used. Targets for these models included oxalate, carbonate, nitrite, hydroxide, and phosphate, utilizing 30 of the most similar spectra in the PLS model. The number of latent variables (LVs) was optimized for each analyte based on the number of components required to capture the signal of each analyte. Spectra were preprocessed by applying the first derivative, normalizing to the water band, and then applying a mean centering before further analysis. Cross validation was completed using venetian blinds with 10 data splits and 1 sample per blind. In all models, each analyte was modeled separately using a limited spectral range, which encompassed only the spectral signature range for each analyte.

By doing this, the model is better able to ignore contributions from other analytes. Two overall approaches were utilized: (1) individual models were made for each laser system and (2) multiblock models were made that simultaneously utilized data from all three Raman systems.[29]

In the first modeling method, each laser system was analyzed separately; this provides a comparison of the effectiveness of each laser system in measuring each analyte. Example modeling results are shown in Figure 4, including analytes with a strong response (nitrate) and weak response (oxalate). An example loadings plot for the 532 nm system is included in Figure S5 comparing the number of LVs needed for nitrate, chromate, and oxalate. More LVs were needed to capture the spectral variation caused by oxalate due to the relatively low signal and interfering overlapping bands. Also shown is one of the interesting exceptions to the general trend of better performance by the blue system: chromate. Model statistics included the root-mean-square error of calibration (RMSEC), which is a

https://doi.org/10.1021/acsestwater.1c00408
ACS EST Water XXXX, XXX, XXX–XXX

Table 3. Modeling Statistics for Nitrate, Chromate, and Oxalate Comparing Multiblock Modeling with Each Separate Model for the 405, 532, and 671 nm Systems

analyte	LVs	model (nm)	RMSEC (M)	RMSECV (M)	R^2 (cal)	R^2 (CV)
NO_3^-	2	405	0.0283	0.0339	0.996612	0.99558
	2	532	0.0232	0.0386	0.99724	0.99931
	2	671	0.0267	0.0379	0.99697	0.994171
	2	multiblock	0.0272	0.0382	0.99688	0.99398
CrO_4^{2-}	2	405	0.0311	0.0865	0.952595	0.652312
	2	532	0.00341	0.00530	0.999423	0.998398
	2	671	0.00344	0.00573	0.999423	0.998398
	2	multiblock	0.00322	0.00578	0.99949	0.99837
$C_2O_4^{2-}$	3	405	0.0000481	0.0188	0.999993	0.488593
	3	532	0.0000389	0.000555	0.999996	0.999173
	3	671	0.000272	0.00221	0.999791	0.988088
	3	multiblock	0.000539	0.00474	0.99917	0.93767

measure of the model's ability to predict the known concentrations of the training set, the root-mean-square error of cross validation (RMSECV), which is a measure of model's ability to predict concentrations of training set data left out of the model during cross validation, and the root-mean-square error of prediction (RMSEP), which is a measure of the model's ability to predict concentrations of validation set samples not included in the training set. The statistics for RMSEC and RMSECV for these models are shown in Table 3. With the large error associated with the concentrations of the real processing samples (15%) and with some analyte concentrations entirely unknown, the RMSEP values calculated for these samples do not serve as a reliable basis for measuring the error associated with the model. Therefore, the RMSEP was not considered when discussing model performance.

The second modeling method focused on combining all laser data together into a multiblock model. Example results for these multiblock models for nitrate, chromate, and oxalate are shown in Figure 5, and the modeling statistics are presented in Table 3. Parity plots for all analytes using multiblock modeling are included in Figure S6, and associated modeling statistics are included in Table S4. Using this method, models can compensate for weaknesses of specific laser systems by emphasizing other laser system data. For example, the 405 nm excitation wavelength is absorbed by yellow chromate solutions, resulting in a loss of signal produced by that laser system. This can be seen in Table 3, where multiblock models have comparable model metrics to single-wavelength models but can be applied to a wider range of analytes as demonstrated by the improved metrics for the multiblock model of CrO_4^{2-} compared to the 405 nm system. Note, RMSECV values can roughly be interpreted as uncertainty, or ± M values, on model outputs.[30] Here, comparing RMSECV values to limits of detection in Table 2 help provide some insight into the utility of these approaches at very low concentrations.

Application to Real-Waste Samples. Several real-waste processing samples were available for spectral collection and application of chemometric models. This included very low-concentration streams representing the condensate from glass melting operations. Figure 6 provides examples of spectral responses from two of these samples, and spectra for all of the real-waste samples are shown in Figure S8. Note, to fully characterize model accuracy, a variety of simulants were included along with real tank processing samples within the validation set. These included tank simulant samples and

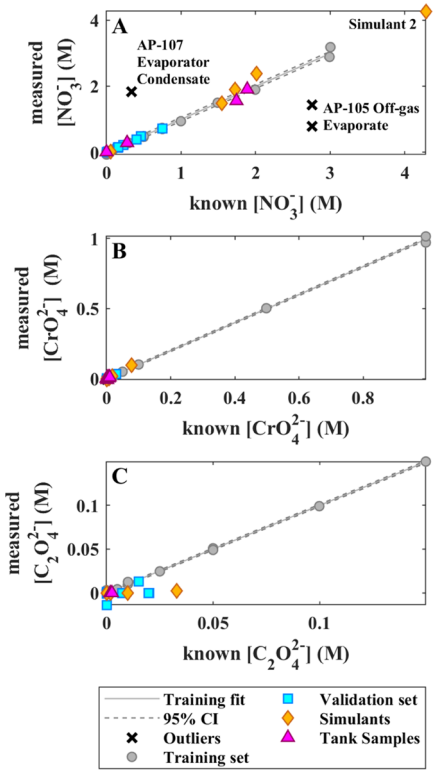

Figure 5. Parity plots built using multiblock modeling showing examples of nitrate (A), chromate (B), and oxalate (C) models.

additional validation samples with low concentrations of analytes. Note, for nonradioactive samples prepared for the training set, validation, and simulant samples, "known" concentrations were determined by dilution of volumetrically prepared stock samples. For tank samples, "known" concentrations were determined by either ion chromatography (IC), inductively coupled plasma optical emission spectrometry (ICP-OES), or acid/base titration for hydroxide concentration. The error associated with the tank sample analyses is generally reported as 15%.

Overall, significant spectral complexity was exhibited by simulants and especially real tank samples. Model performance was overall excellent in handling these samples. This can be seen in Figures 4, 5, and S6, which include results on the parity plots. Notable exceptions can be seen in Figure 5A, where the nitrate predicted value was too high for the AP-107 evaporator

https://doi.org/10.1021/acsestwater.1c00408
ACS EST Water XXXX, XXX, XXX−XXX

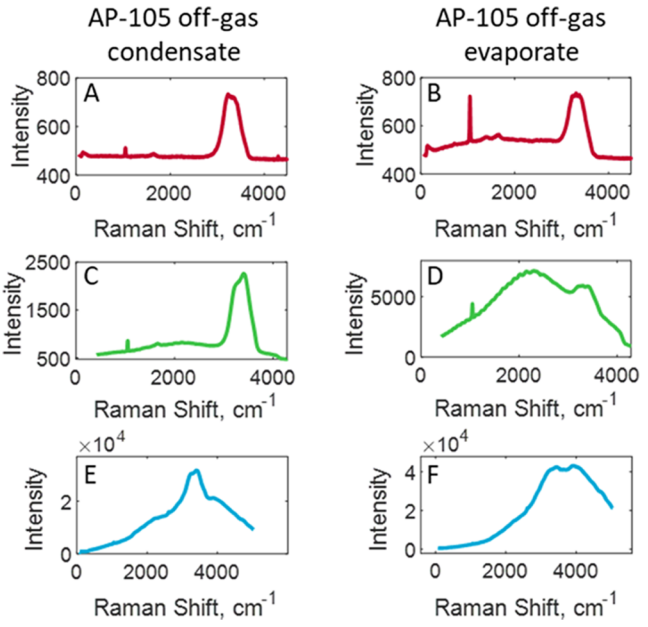

Figure 6. Example Raman spectra of AP-105 off-gas samples including condensate (A, C, E) and evaporate (B, D, F) samples measured by 671 nm (A, B), 532 nm (C, D), and 405 nm (E, F) systems. Each spectrum represents an average of 200 spectra with an integration time of 0.1 s. The spectra in this figure have been replotted on a common wavelength (absolute nm) scale to highlight the differences in Raman spectra collected with different wavelengths of excitation and are shown in Figure S7.

condensate sample and too low for the two measurements of the AP-105 off-gas evaporate sample (shown as X's). This may actually be a valuable result indicating that the known values may be incorrect due to either analysis errors or transcription errors or that the samples may have precipitated during the wait time between sample generation/offline characterization and spectral collection of Raman data. While these results do not prove that the known concentrations are incorrect, significant outliers can indicate that a sample concentration is, in fact, different than the expected value and can be a valuable indication of off-normal events.

The process sample spectra shown in Figures 6 and S8 also show a notable observed fluorescence of some tank processing samples that interfere with the blue and, to a lesser extent, the green Raman systems. This highlights the tradeoff between improved sensitivity at lower excitation wavelengths (see Table 2) and increased potential for interfering fluorescence (see Figure 6). In all cases observed here, fluorescence was not significant enough in the green system to impact results but was significant enough on the blue system to interfere with model performance.

While fluorescence is generally considered to be independent of excitation, this rule of thumb is for systems where the change in excitation wavelength is relatively small ($\Delta\lambda_{ex}$ < 10 nm), and if there is only one emissive component within the sample. In addition, it is generally accepted that wavelength-dependent fluorescence involves emission from multiple states of difference conformers of a single molecule or from different molecules.[31] In our case, the λ_{ex} difference between the 405, 532, and 671 nm wavelengths is quite large, having $\Delta\lambda_{ex}$ of 127 nm (532−405 nm), 139 nm (671−532 nm), and 266 nm (671−405 nm), thus enabling the excitation into different electronic manifolds of various organic constituents within the actual waste samples. Since this phenomenon was not observed in the prepared standards (Figures 2 and 3), which are relatively simple in composition and contain a limited number of known constituents and was only observed in the actual waste-derived samples (Figure 6), we assume the fluorescence is derived from the complexity of the actual waste. The spectral measurements shown in Figures 6 and S8 consist of radioactive waste samples from Hanford tanks AP-105, AP-107, and AW-102, resulting from 5 to 6 decades of active accumulation of waste constituents during radioactive waste management at the Hanford site.[1] The organic constituents within this waste are complex and varied and are an accumulation of solvents (dodecane, kerosine, etc.), extractants (tri-butyl-phosphate (TBP), etc.), complexants (citrate, glycolate, EDTA, etc.), and other industrial inorganic and organic wastes, which have been made more complex in nature by the thermal and radiolytic digestion of the parent organic reagents in contact with highly concentrated brines (salts of NO_3^-, NO_2^-, SO_4^{2-}, OH^-, $Al(OH)_4^-$, etc.).[1] To clearly show the wavelength dependence, we have replotted the Raman spectra in Figure 6 on an absolute wavelength scale (Raman intensity vs nm), shown in Figure S7. A broad band emission is seen in the spectra of actual waste shown in these figures, which is more prevalent at lower wavelength excitation than at longer, with decreasing emission with excitation wavelengths in the order 405 > 532 > 671 nm.

In addition to parity plots in Figures 4 and 5, model performance can be characterized by looking at Q residuals and hotelling T^2 residuals.[32−34] Figure 7 presents examples of model metrics for the nitrate, chromate, and oxalate multiblock models. Here, again the AP-105 off-gas evaporate sample shows high Q and T^2 values for both chromate and oxalate, indicating that the sample concentrations are outside the bounds of the model training set. Also noted in Figures 5 and 7

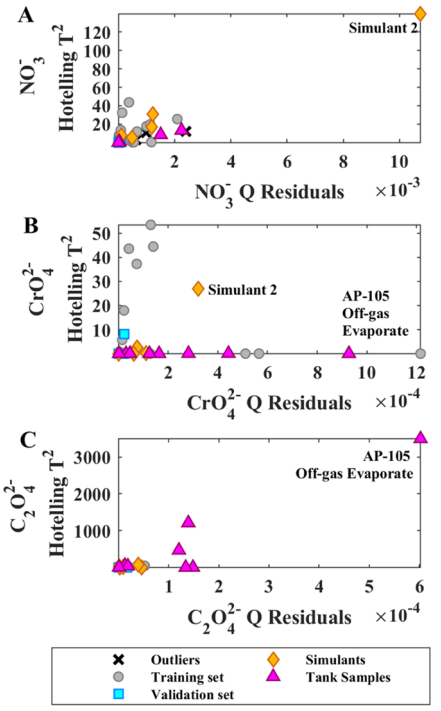

Figure 7. Q residuals vs hotelling T^2 for nitrate (A), chromate (B), and oxalate (C) from multiblock models.

https://doi.org/10.1021/acsestwater.1c00408
ACS EST Water XXXX, XXX, XXX−XXX

is Simulant 2 (S-109 early feed), which shows high Q and T^2 values for both nitrate and chromate, indicating that this sample fell outside the range of what the model had seen before. Figure 5A demonstrates this where the Simulant 2 sample had a nitrate concentration that was higher than the training set range but still fell within the expected linear trend, indicating that the model was still able to accurately quantify the nitrate concentration of this sample. This is an indication of the model's robustness in accurately predicting concentrations outside the range in which the model was built.

Overall, after optimizing collection parameters for single Raman excitation wavelength systems, model performance is roughly comparable between the 405, 532, and 671 nm systems based on RMSECV. If targeting specific analytes, e.g., chromium, that have absorption or fluorescence challenges, it may be better to choose one system over the other, e.g., 532 over 405 nm for chromium. In terms of the greatest overall improvement, multiblock modeling allowed for models that improved general applicability (i.e., lower RMSECV values) across a wide range of analytes.

CONCLUSIONS

Raman spectroscopy combined with chemometric modeling performed well in characterizing low-concentration samples. This was primarily due to optimizing instrument specifications such as excitation wavelength, collection time, or spectral averaging. Here, three Raman systems were utilized including the 671, 532, and 405 nm systems. Improved sensitivity was observed at lower excitation wavelengths, but higher fluorescence from real Hanford tank processing samples was also observed. Chemometric models utilizing multiblock approaches (simultaneously using data from all three Raman systems) performed well and provided improved robustness in the face of fluorescence or spectral interferences. Low limits of detection and low uncertainties (measured as the root-mean-square error of cross validation, RMSECV) all suggested further successful application to low-concentration process streams. Overall, results observed here show the successful application of Raman-based monitoring approaches to the analysis of low-concentration Hanford processing streams, suggesting that the benefits of process monitoring can be leveraged in a variety of Hanford processing conditions.

ASSOCIATED CONTENT

Supporting Information

The Supporting Information is available free of charge at https://pubs.acs.org/doi/10.1021/acsestwater.1c00408.

Details of Raman spectroscopy performance from multiple Raman systems under a variety of collection parameters and information on chemometric modeling and model results (PDF)

AUTHOR INFORMATION

Corresponding Authors

Samuel A. Bryan − *Pacific Northwest National Laboratory, Richland, Washington 99352, United States;* orcid.org/0000-0002-8826-0880; Phone: (509) 375-5648; Email: sam.bryan@pnnl.gov

Amanda M. Lines − *Pacific Northwest National Laboratory, Richland, Washington 99352, United States*; Phone: (509) 375-5689; Email: amanda.lines@pnnl.gov

Authors

Heather M. Felmy − *Pacific Northwest National Laboratory, Richland, Washington 99352, United States*

Hope E. Lackey − *Pacific Northwest National Laboratory, Richland, Washington 99352, United States*

Adan Schafer Medina − *Pacific Northwest National Laboratory, Richland, Washington 99352, United States*

Michael J. Minette − *Pacific Northwest National Laboratory, Richland, Washington 99352, United States*

Complete contact information is available at: https://pubs.acs.org/10.1021/acsestwater.1c00408

Notes

The authors declare no competing financial interest.

ACKNOWLEDGMENTS

We thank Michael C. Perkins for graphic design assistance. Research was supported by U.S. Department of Energy, Office of Environmental Management, through the Office of River Protection and was performed at the Pacific Northwest National Laboratory (PNNL) operated by Battelle for the U.S. Department of Energy under Contract DE-AC05-76RL01830.

REFERENCES

(1) Gephart, R. E.; Lundgren, R. E. *Hanford Tank Clean up: A Guide to Understanding the Technical Issues*, 3rd ed.; Pacific Northwest National Laboratory: Richland, Washington, 1995; Vol. *27*.

(2) Beer, T. D.; Burggraeve, A.; Fonteyne, M.; Saerens, L.; Remon, J. P.; Vervaet, C. Near infrared and Raman spectroscopy for the in-process monitoring of pharmaceutical production processes. *Int. J. Pharm.* **2011**, *417*, 32−47.

(3) Leersnyder, F. D.; Peeters, E.; Djalabi, H.; Vanhoorne, V.; Snick, B. V.; Hong, K.; Hammond, S.; Liu, A. Y.; Ziemons, E.; Vervaet, C.; Beer, T. D. Development and validation of an in-line NIR spectroscopic method for continuous blend potency determination in the feed frame of a tablet press. *J. Pharm. Biomed. Anal.* **2018**, *151*, 274−283.

(4) Bogomolov, A.; Dietrich, S.; Boldrini, B.; Kessler, R. W. Quantitative determination of fat and total protein in milk based on visible light scatter. *Food Chem.* **2012**, *134*, 412−418.

(5) Rodionova, O. Y.; Pomerantsev, A. L. Non-linear multivariate curve resolution applied to the spectrophotometric determination of cerium(III) in aqueous nitric acid solutions for process control. *Anal. Methods* **2016**, *8*, 435−444.

(6) Rodionova, O. Y.; Titova, A. V.; Demkin, N. A.; Balyklova, K. S.; Pomerantsev, A. L. Qualitative and quantitative analysis of counterfeit fluconazole capsules: A non-invasive approach using NIR spectroscopy and chemometrics. *Talanta* **2019**, *195*, 662−667.

(7) Bryan, S. A.; Levitskaia, T. G.; Johnsen, A. M.; Orton, C. R.; Peterson, J. M. Spectroscopic monitoring of spent nuclear fuel reprocessing streams: an evaluation of spent fuel solutions via Raman, visible, and near-infrared spectroscopy. *Radiochim. Acta* **2011**, *99*, 563−571.

(8) Casella, A. J.; Ahlers, L. R. H.; Campbell, E. L.; Levitskaia, T. G.; Peterson, J. M.; Smith, F. N.; Bryan, S. A. Development of Online Spectroscopic pH Monitoring for Nuclear Fuel Reprocessing Plants: Weak Acid Schemes. *Anal. Chem.* **2015**, *87*, 5139−5147.

(9) Nelson, G. L.; Lackey, H. E.; Bello, J. M.; Felmy, H. M.; Bryan, H. B.; Lamadie, F.; Bryan, S. A.; Lines, A. M. Enabling Microscale Processing: Combined Raman and Absorbance Spectroscopy for Microfluidic On-Line Monitoring. *Anal. Chem.* **2021**, *93*, 1643−1651.

(10) Tse, P.; Bryan, S. A.; Bessen, N. P.; Lines, A. M.; Shafer, J. C. Review of on-line and near real-time spectroscopic monitoring of processes relevant to nuclear material management. *Anal. Chim. Acta* **2020**, *1107*, 1−13.

(11) Sadergaski, L. R.; DePaoli, D. W.; Myhre, K. G. Monitoring the Caustic Dissolution of Aluminum Alloy in a Radiochemical Hot Cell Using Raman Spectroscopy. *Appl. Spectrosc.* **2020**, *74*, 1252−1262.
(12) Sadergaski, L. R.; Toney, G. K.; Delmau, L. H.; Myhre, K. G. Chemometrics and Experimental Design for the Quantification of Nitrate Salts in Nitric Acid: Near-Infrared Spectroscopy Absorption Analysis. *Appl. Spectrosc.* **2021**, *75*, 1155−1167.
(13) Clifford, A. J.; Lackey, H. E.; Nelson, G. L.; Bryan, S. A.; Lines, A. M. Raman Spectroscopy Coupled with Chemometric Analysis for Speciation and Quantitative Analysis of Aqueous Phosphoric Acid Systems. *Anal. Chem.* **2021**, *93*, 5890−5896.
(14) Lackey, H. E.; Nelson, G. L.; Lines, A. M.; Bryan, S. A. Reimagining pH Measurement: Utilizing Raman Spectroscopy for Enhanced Accuracy in Phosphoric Acid Systems. *Anal. Chem.* **2020**, *92*, 5882−5889.
(15) Myhre, K. G.; Mehta, M. J.; Martin, M. Z.; Du, M. T. Laser Induced Breakdown Spectroscopy analysis of europium and samarium in aluminum oxide. *Spectrochim. Acta B* **2018**, *149*, 30−34.
(16) Nelson, G. L.; Asmussen, S. E.; Lines, A. M.; Casella, A. J.; Bottenus, D. R.; Clark, S. B.; Bryan, S. A. Micro-Raman Technology to Interrogate Two-Phase Extraction on a Microfluidic Device. *Anal. Chem.* **2018**, *90*, 8345−8353.
(17) Felmy, H. M.; Clifford, A. J.; Medina, A. S.; Cox, R. M.; Wilson, J. M.; Lines, A. M.; Bryan, S. A. On-Line Monitoring of Gas-Phase Molecular Iodine Using Raman and Fluorescence Spectroscopy Paired with Chemometric Analysis. *Environ. Sci. Technol.* **2021**, *55*, 3898−3908.
(18) Schroll, C. A.; Lines, A. M.; Heineman, W. R.; Bryan, S. A. Absorption spectroscopy for the quantitative prediction of lanthanide concentrations in the 3LiCl-2CsCl eutectic at 723 K. *Anal. Methods* **2016**, *8*, 7731−7738.
(19) Lines, A. M.; Tse, P.; Felmy, H. M.; Wilson, J. M.; Shafer, J.; Denslow, K. M.; Still, A. N.; King, C.; Bryan, S. A. Online, Real-Time Analysis of Highly Complex Processing Streams: Quantification of Analytes in Hanford Tank Sample. *Ind. Eng. Chem. Res.* **2019**, *58*, 21194−21200.
(20) Bryan, S. A.; Levitskaia, T. G.; Sinkov, S. I.; Schlahta, S. N.; Shaver, J. M. In *Raman Based Process Monitor for Continuous Real-Time Analysis of High Level Radioactive Waste Components*, Abstracts of Papers of the American Chemical Society, 2006; Vol.232, 852.
(21) Lines, A. M.; Nelson, G. L.; Casella, A. J.; Bello, J. M.; Clark, S. B.; Bryan, S. A. Multivariate Analysis To Quantify Species in the Presence of Direct Interferents: Micro-Raman Analysis of HNO3 in Microfluidic Devices. *Anal. Chem.* **2018**, *90*, 2548−2554.
(22) Nelson, G. L.; Lines, A. M.; Casella, A. J.; Bello, J. M.; Bryan, S. A. Development and testing of a novel micro-Raman probe and application of calibration method for the quantitative analysis of microfluidic nitric acid streams. *Analyst* **2018**, *143*, 1188−1196.
(23) Harris, D. C. *Quantitative Chemical Analysis*, 7th; W.H. Freeman and Co.: New York, NY, 2007.
(24) Kiefer, W.; Bernstein, H. J. The resonance Raman effect of the permanganate and chromate ions. *Mol. Phys.* **1972**, *23*, 835−851.
(25) Casella, A.; Lines, A.; Nelson, G.; Bello, J.; Bryan, S. MicroRaman Measurements for Nuclear Fuel Reprocessing Applications. *Procedia Chem.* **2016**, *21*, 466−472.
(26) Beebe, K. R.; Pell, R. J.; Seasholtz, M. B. *Chemometrics: A Practical Guide*; Wiley: New York,1998.
(27) Bro, R.; Eldén, L. PLS works. *J. Chemom.* **2009**, *23*, 69−71.
(28) Lines, A. M.; Adami, S. R.; Sinkov, S. I.; Lumetta, G. J.; Bryan, S. A. Multivariate Analysis for Quantification of Plutonium(IV) in Nitric Acid Based on Absorption Spectra. *Anal. Chem.* **2017**, *89*, 9354−9359.
(29) Skov, T.; Ballabio, D.; Bro, R. Multiblock variance partitioning: A new approach for comparing variation in multiple data blocks. *Anal. Chim. Acta* **2008**, *615*, 18−29.
(30) Faber, N. K. M.; Bro, R. Standard error of prediction for multiway PLS 1. Background and a simulation study. *Chemom. Intell. Lab. Syst.* **2002**, *61*, 133−149.
(31) Józefowicz, M.; Heldt, J. R. Excitation-wavelength Dependent Fluorescence of Ethyl 5-(4-aminophenyl)-3-amino-2,4-dicyanobenzoate. *J. Fluoresc.* **2011**, *21*, 239−245.
(32) Mujica, L. E.; Rodellar, J.; Fernández, A.; Güemes, A. Q-statistic and T2-statistic PCA-based measures for damage assessment in structures. *Struct. Health Monit.* **2011**, *10*, 539−553.
(33) Wise, B. M.; Gallagher, N. B. The process chemometrics approach to process monitoring and fault detection. *J. Process Control* **1996**, *6*, 329−348.
(34) Potyrailo, R. A. On-line Measurement. In *Encyclopedia of Materials: Science and Technology*; Buschow, K. H. J.; Cahn, R. W.; Flemings, M. C.; Ilschner, B.; Kramer, E. J.; Mahajan, S.; Veyssière, P., Eds.; Elsevier: Oxford, 2001; pp 6401−6411.

https://doi.org/10.1021/acsestwater.1c00408
ACS EST Water XXXX, XXX, XXX−XXX